

# Darwin-Vlasov Simulations of magnetized Plasmas

H. Schmitz and R. Grauer

*Theoretische Physik I, Ruhr-Universität Bochum, 44780 Bochum, Germany*

---

## Abstract

We present a new Vlasov code for collisionless plasmas in the nonrelativistic regime. A Darwin approximation is used for suppressing electromagnetic vacuum modes. The spatial integration is based on an extension of the flux-conservative scheme, introduced by Filbet et al. [23]. Performance and accuracy is demonstrated by comparing it to a standard finite differences scheme for two test cases, including a Harris sheet magnetic reconnection scenario. This comparison suggests that the presented scheme is a promising alternative to finite difference schemes.

*Key words:* Vlasov simulations, positive flux-conservative scheme, Darwin approximation, Boris scheme, reconnection

*PACS:* 02.70.-c, 52.25.Dg, 52.65.Ff, 52.25.Xz, 52.35.Vd

---

## 1 Introduction

For many interesting problems in plasma physics a deeper understanding can only be gained with the help of kinetic plasma models. In contrast to macroscopic models where only the streaming velocity, pressure, temperature and other fluid quantities are considered, the kinetic description deals with the particle distribution function  $f(\mathbf{x}, \mathbf{v})$ . Here  $\mathbf{x}$  is the position in space and  $\mathbf{v}$  is the three dimensional velocity. The equation describing the evolution of the six dimensional distribution function in phase space for a collisionless system is the Vlasov equation. The complexity of kinetic plasma descriptions arises because of the electromagnetic fields appearing in the Vlasov equation. These depend on the charge density and current density in the plasma which are in turn given by the moments of the distribution function. Thus the system presents itself as a strongly coupled non-linear system of partial differential equations. Analytical solutions of this system are only possible for a very restricted number of special problems.

Among the numerous problems, where collisionless kinetic plasma simulations are important, we name only two topics, which are important in both laboratory- and astrophysical settings. These are the thin current sheet region in collisionless magnetic reconnection processes and the structure of collisionless shocks. The Harris sheet model [1] gives a kinetic equilibrium of a current sheet separating two regions of different magnetic field. While this can be formulated analytically, the reconnection process, which is initiated by small perturbations from the Harris equilibrium, is not yet fully understood. Also, there has been tremendous progress in the last 10 years, both on the fluid level (see [2,3,4,5,6,7]) and using kinetic simulations (see [8,9,10,11,12,13,14,15,16,17] for Particle in Cell simulations and [18,19] for Vlasov simulations). Still many questions remain to be solved, such as: the spontaneous onset of reconnection, three dimensional effects, turbulence in the reconnection zone, acceleration of particles, and comparison to experiments. It has become clear that, especially for the acceleration of particles, fully kinetic models and simulations are inevitable. Up to now most kinetic simulations make use of the Particle in Cell method (PIC), and very few deal with a direct integration of the Vlasov equation. In order to validate PIC simulations of collisionless magnetic reconnection, it is necessary to simulate the same problems using different schemes, and Vlasov schemes are an important alternative method.

The second important system currently investigated is the problem of collisionless shocks. In the framework of MHD-equations these shocks appear as singular points, where the macroscopic quantities show a discontinuity. To understand the inner structure of shocks, kinetic models are necessary since only they can describe the underlying dissipation processes. For some special geometries together with low Mach numbers there are time independent analytical solutions to the kinetic equations, corresponding to stable shock conditions. For higher Mach numbers these solutions break down, and a time dependant behaviour appears. This leads to excitation of wave modes with a possibility of particle acceleration. This time dependant behaviour is not accessible with analytical methods, and numerical approaches have to be attempted.

As mentioned above, in practise there are two different numerical approaches to solving the Vlasov equation. In the Particle in Cell (PIC) approach trajectories of individual representative particles are followed through the electromagnetic fields. The fields are given on a numerical grid, while the positions and velocities of the simulation particles can be any value. Due to the finite number of particles, the PIC method suffers from considerable numerical noise. A related problem is the fact that only those parts of the distribution function can be calculated with high precision which contain many particles in a phase space volume. In particular the high energy tails of the distribution function cannot be resolved.

The other numerical approach integrates the Vlasov equation directly on a high dimensional numerical grid in phase space. These Vlasov schemes do not suffer from any numerical noise. The tails of the distribution function can be modelled with high accuracy, and deviations from a Maxwellian distribution can be pinpointed. These advantages are traded against higher computational effort of the Vlasov–codes as compared to PIC–codes. Additionally, care has to be taken for choosing the integration scheme of Vlasov’s equation, taking into account the hyperbolic nature and corresponding integral quantities.

The distribution function has to fulfil a number of restrictions which are derived from its physical interpretation as probability density in phase space and from the properties of the Vlasov equation. The probability density interpretation implies that the distribution function has to remain positive at all times. One property of Vlasov’s equation is that the values of the distribution function are transported along the characteristics through phase space without modification. When starting from a positive distribution function this not only implies that the positivity is preserved but also that both upper and lower bounds of the distribution function remain unchanged, and that no new maxima or minima are generated. A second property of Vlasov’s equation is the conservation of phase space density as a consequence of Liouville’s equation.

A numerical scheme cannot satisfy all the above criteria exactly. Therefore a number of numerical schemes have been proposed, each of which is a compromise between different requirements. Spectral codes which solve the Vlasov equation in the Fourier domain suffer only from little numerical diffusion, but they are mostly limited to periodic boundary conditions, see e.g. [21]. Another important drawback of these methods is that they do not preserve positivity, let alone the number of extrema in the distribution function. Eulerian solvers, on the other hand, allow for non–periodic boundary conditions and can be made to preserve positivity and the maximum principle. They are, however, slightly more diffusive than spectral codes. A recent comparison of Eulerian solvers can be found in [22]. In this work we will use a flux conservative and positive scheme [23] which obeys the maximum principle and suffers from relatively little numerical diffusion.

The integration of the Vlasov equation has to be performed simultaneously to the evaluation of the Maxwell equations. The dynamics of the full electrodynamic fields imposes an additional criterion for the time step used in the simulation. Since electromagnetic waves can travel through the system, the time step has to be chosen such that the speed of light  $c$  is resolved on the numerical grid:  $\Delta t < c\Delta x$ , where  $\Delta t$  is the time step and  $\Delta x$  is the grid resolution. One way to avoid this is to use an electrostatic model. This is, however, only applicable in special situations where the self generated magnetic field can be neglected. Here we will use the Darwin approximation of Maxwell’s equations, which follows from a rigorous expansion of the full Maxwell equa-

tions in orders of  $v^2/c^2$ , where  $v$  is a characteristic velocity of the system. In the framework of the Darwin approximation, the purely electromagnetic modes are neglected but electrostatic, magnetostatic, and inductive fields are still considered. Darwin's approximation has been widely used with Particle in Cell simulations [24,27], however, it has not found its way into Vlasov simulations yet. An alternative method is the use of an implicit time stepping as it has been implemented by [14] in the Celested3D code.

The next section will present the basic equations together with their normalisation. In section 3 we will introduce the Darwin approximation of the Maxwell equations. Section 4 will give an overview of the one dimensional flux conservative scheme used for integrating Vlasov's equation, while section 5 will describe the time splitting schemes that provides the generalisation to the 5-dimensional phase space. In section 6 results are presented, and section 7 contains some concluding remarks.

## 2 Basic equations

In this and the next section we want to present the basic equations and approximations of our model. The aim is to simulate Vlasov's equation

$$\frac{\partial f_k}{\partial t} + \mathbf{v} \cdot \nabla f_k + \frac{q_k}{m_k} (\mathbf{E} + \mathbf{v} \times \mathbf{B}) \cdot \nabla_{\mathbf{v}} f_k = 0.$$

Here  $f_k(\mathbf{x}, \mathbf{v}, t)$  is the distribution function of species  $k$ . In this work only singly charged ions and electrons  $k = i, e$  are considered, although the code allows arbitrary species. The quantities  $q_k$  and  $m_k$  are the charge and the mass of the particles of species  $k$ . The Lorentz force depends on the electric and magnetic fields. These are in general given by Maxwell's equations,

$$\nabla \times \mathbf{E} = -\frac{\partial \mathbf{B}}{\partial t} , \tag{1}$$

$$\frac{1}{\mu_0} \nabla \times \mathbf{B} = \varepsilon_0 \frac{\partial \mathbf{E}}{\partial t} + \mathbf{j} , \tag{2}$$

$$\nabla \cdot \mathbf{E} = \frac{1}{\varepsilon_0} \rho , \tag{3}$$

$$\nabla \cdot \mathbf{B} = 0 , \tag{4}$$

where  $\mathbf{B}$  is the magnetic and  $\mathbf{E}$  the electric field. In section 3 we will present the Darwin approximation of Maxwell's equations, which is used to solve the electromagnetic fields in our simulation code. The charge density  $\rho$  and the

current density  $\mathbf{j}$  are given by the moments of the distribution function,

$$\rho = \sum_k q_k \int f_k(\mathbf{x}, \mathbf{v}) d^3v \quad , \quad (5)$$

$$\mathbf{j} = \sum_k q_k \int \mathbf{v} f_k(\mathbf{x}, \mathbf{v}) d^3v \quad . \quad (6)$$

## 2.1 Normalisation

Here we want to present the normalisation of the Vlasov–Maxwell system equations. For this we introduce normalising parameters  $A_0$ , where  $A$  stands for any of the physical quantities. The normalised quantities  $\hat{A}$  are then given by  $\hat{A} = A/A_0$ .

The un-normalised characteristics of Vlasov’s equation for species  $k$  are given by

$$\frac{d\mathbf{x}}{dt} = \mathbf{v} \quad , \quad (7)$$

$$\frac{d\mathbf{v}}{dt} = \frac{q_k}{m_k} (\mathbf{E} + \mathbf{v} \times \mathbf{B}) \quad . \quad (8)$$

Here we have used the symbols  $\mathbf{x}$  and  $\mathbf{v}$  to denote the characteristics  $\mathbf{x} = \mathbf{x}(t, \mathbf{x}_0, \mathbf{v}_0)$  and  $\mathbf{v} = \mathbf{v}(t, \mathbf{x}_0, \mathbf{v}_0)$ . These have to be distinguished from the independent variables  $\mathbf{x}$  and  $\mathbf{v}$  in Vlasov’s equation. In the following the appropriate meaning should be clear from the context. The form of the above equations is not modified by the normalisation,

$$\frac{d\hat{\mathbf{x}}}{d\hat{t}} = \hat{\mathbf{v}} \quad , \quad (9)$$

$$\frac{d\hat{\mathbf{v}}}{d\hat{t}} = \frac{\hat{q}_k}{\hat{m}_k} (\hat{\mathbf{E}} + \hat{\mathbf{v}} \times \hat{\mathbf{B}}) \quad . \quad (10)$$

Only the individual charge to mass ratios  $\hat{q}_k/\hat{m}_k$  are relevant parameters of the system. On the other hand, Maxwell’s equations simplify to

$$\nabla \times \hat{\mathbf{E}} = -\frac{\partial \hat{\mathbf{B}}}{\partial \hat{t}} \quad , \quad (11)$$

$$\nabla \times \hat{\mathbf{B}} = \alpha^2 \left( \frac{\partial \hat{\mathbf{E}}}{\partial \hat{t}} + \hat{\mathbf{j}} \right) \quad , \quad (12)$$

$$\nabla \cdot \hat{\mathbf{E}} = \hat{\rho} \quad , \quad (13)$$

$$\nabla \cdot \hat{\mathbf{B}} = 0 \quad . \quad (14)$$

Here  $\alpha = v_0/c$  is the ratio of the normalisation velocity over the speed of light.

We choose  $m_0 = m_i$  and  $q_0 = e$ , where  $m_i$  is the ion mass and  $e$  is the unit electron charge.  $B_0$  and  $n_0$  remain free to choose. Then  $x_0 = \lambda_i$  is the ion inertial length,  $t_0 = 1/\Omega_i$  is the inverse ion gyro frequency ( $\Omega_i = \frac{eB}{m_i}$ ), and  $v_0 = v_A = B_0/\sqrt{\mu_0 m_i n_0}$  is the Alfvén velocity.

We still have the freedom of choosing the magnetic field  $B_0$ . If we choose  $B_0$  to be a characteristic magnetic field magnitude in the system, then  $\alpha$  gives the ratio of Alfvén velocity to the speed of light in the system. On the other hand we can choose  $B_0$  such that  $\alpha = 1$ . Then the local magnetic field magnitude in the system determines  $v_A/c$ . In this work we will choose the first, so that the field magnitude in the system remains around unity and the free parameter  $\alpha$  can be used to set the magnetic field strength. In the following we will drop the hat-notation ( $\hat{\phantom{x}}$ ) for the normalised quantities.

### 3 Darwin approximation

The flux conservative integration scheme of the Vlasov equation, which will be presented in section 4, is not restricted by a CFL condition on the time step. However, when combined with the Maxwell equations for the electromagnetic fields a CFL condition is introduced by the time integration of the fields on the numerical grid. This implies that the fastest electromagnetic wave mode, i.e. the vacuum mode, has to be resolved on the grid,

$$\Delta t < \frac{\Delta x}{c} , \quad (15)$$

where  $c$  is the speed of light. This condition imposes severe restrictions on the time step. In many applications the electromagnetic vacuum modes are not important. The standard solution to this problem is the electrostatic approximation. In this approximation only Poisson’s equation needs to be solved for the electric field. A magnetic vacuum field can also be superimposed. The influence of the plasma on the magnetic field is, however, completely neglected. To account for this influence, and thus the possibility of magnetosonic wave modes, the Darwin approximation is commonly used in particle simulations. This approximation can be derived from the Maxwell equations in an expansion in orders of  $v^2/c^2$ , where  $v$  is some characteristic velocity. Assuming  $v^2 \ll c^2$  this leads to a set of equations where the vacuum modes are eliminated but all other wave modes are retained. Darwin’s approximation can be used when the velocities are small compared to the speed of light and there is no energy transported by the electromagnetic radiation. Some applications are the study of magnetic reconnection, e.g. in the earths magnetotail [25], or the investigation of high intensity charged particle beams [26]. Naturally it is not capable of describing phenomena where the electromagnetic vacuum modes play a major role, e.g. in laser–plasma interaction.

Darwin's approximation starts from a separation of the electric field into a longitudinal and a transverse part [27]

$$\mathbf{E} = \mathbf{E}_L + \mathbf{E}_T \quad , \quad (16)$$

with

$$\nabla \times \mathbf{E}_L = 0 \quad \text{and} \quad \nabla \cdot \mathbf{E}_T = 0 \quad . \quad (17)$$

The normalised Maxwell's equations are then approximated by

$$\nabla \cdot \mathbf{E}_L = \rho \quad , \quad (18)$$

$$\nabla \cdot \mathbf{B} = 0 \quad (19)$$

$$\nabla \times \mathbf{E}_T = -\partial_t \mathbf{B} \quad , \quad (20)$$

$$\nabla \times \mathbf{B} = \alpha^2 (\partial_t \mathbf{E}_L + \mathbf{j}) \quad . \quad (21)$$

The approximation only appears in eq (21), where only the longitudinal part of the displacement current is taken. All other equations remain unchanged. In vacuum, equations (20) and (21) are now decoupled and no purely electromagnetic modes can appear.

An advantage of using Darwin's approximation instead of the full Maxwell equations is the fact, that the equations can be solved without performing a time integration step. All the electromagnetic fields can be calculated from the moments of the distribution at a given time together with the boundary conditions for the fields. This will be presented in the following.

Poisson's equation for the electrostatic potential

$$\Delta \Phi = -\rho \quad \text{with} \quad \mathbf{E}_L = -\nabla \Phi$$

immediately gives the longitudinal electric field. Taking the curl of (21), together with (17) and (19), results in

$$\Delta \mathbf{B} = -\alpha^2 \nabla \times \mathbf{j} \quad ,$$

giving three Poisson equations for the components of the magnetic field. To calculate  $\mathbf{E}_T$  the curl of eq (20) is taken and eqs (21) and (17) substituted, giving

$$\Delta \mathbf{E}_T = \partial_t \nabla \times \mathbf{B} \quad (22)$$

$$= \alpha^2 \partial_t \mathbf{j} - \nabla (\alpha^2 \partial_t \phi) \quad . \quad (23)$$

To eliminate the time derivative of the current density,  $\mathbf{j}$  is expressed as moment of the distribution function,

$$\partial_t \mathbf{j} = \sum_k q_k \int \mathbf{v} \partial_t f_k d^3v.$$

Here the index  $k$  sums over all particle species. Now, Vlasov's equations for the different species are substituted,

$$\partial_t \mathbf{j} = - \sum_k \nabla \rho_k \langle \mathbf{v} \mathbf{v} \rangle_k + \sum_k \frac{q_k \rho_k}{m_k} \mathbf{E} + \sum_k \frac{q_k \rho_k}{m_k} \langle \mathbf{v} \rangle_k \times \mathbf{B} .$$

Here the pointed brackets  $\langle \cdot \rangle_k$  denote averaging with the distribution function  $f_k$ . The electric field appearing on the right hand side is, of course, comprised of the longitudinal and the transverse part. While the longitudinal component is already known from the charge density, it is the transverse component that is being calculated here. Inserting  $\partial_t \mathbf{j}$  into eq (23) and introducing the local plasma frequency

$$\omega^2 = \sum_k \frac{q_k \rho_k}{m_k} , \quad (24)$$

this leads to

$$\begin{aligned} \Delta \mathbf{E}_T - \alpha^2 \omega^2 \mathbf{E}_T = \\ - \sum_k \nabla \rho_k \langle \mathbf{v} \mathbf{v} \rangle_k + \sum_k \frac{q_k \rho_k}{m_k} \mathbf{E}_L + \sum_k \frac{q_k \rho_k}{m_k} \langle \mathbf{v} \rangle_k \times \mathbf{B} - \nabla \left( \alpha^2 \partial_{tt} \phi \right) . \end{aligned} \quad (25)$$

This equation is a Helmholtz-equation for each component of  $\mathbf{E}_T$ . The last term on the right hand side can be deduced from the condition  $\nabla \cdot \mathbf{E}_T = 0$ , since it only adds a curl free component to  $\mathbf{E}_T$ . It can thus be omitted to calculate  $\tilde{\mathbf{E}}_T$ , with

$$\Delta \tilde{\mathbf{E}}_T - \alpha^2 \omega^2 \tilde{\mathbf{E}}_T = - \sum_k \nabla \rho_k \langle \mathbf{v} \mathbf{v} \rangle_k + \sum_k \frac{q_k \rho_k}{m_k} \mathbf{E}_L + \sum_k \frac{q_k \rho_k}{m_k} \langle \mathbf{v} \rangle_k \times \mathbf{B} .$$

$\tilde{\mathbf{E}}_T$  is then projected onto its divergence free part by calculating  $\Theta$  with  $\Delta \Theta = \nabla \cdot \tilde{\mathbf{E}}_T$  to give  $\mathbf{E}_T = \tilde{\mathbf{E}}_T - \nabla \Theta$ .

Altogether this sums up to 8 elliptic equations. However, the time spent in solving these equations, compared to the integration of the 5 or 6 dimensional problem, is negligible. This situation is different in PIC simulations. One has to compare about 30 particles per cell used in standard PIC simulations to  $10^3$  -  $30^3$  mesh points for the resolution of the velocity space used in Vlasov codes. For this reason the computational effort of solving the above elliptic equations has an effect on the total computational time in standard PIC simulations, but not in Vlasov simulations.

## 4 Flux Conservative Scheme

In this section we briefly present the numerical scheme used for integrating the Vlasov equation. This scheme has originally been presented in Filbet et



al. [23]. The scheme uses a flux conservative formulation and is based on a third order reconstruction of the primitive of the distribution function using a fixed stencil.

To formulate the scheme we start from the observation that in Hamiltonian systems the values of the distribution function are transported along the characteristics

$$f(\xi, t) = f(X(s, t, \xi), s). \quad (26)$$

Here  $X(s, t, \xi)$  denotes the characteristic with parameter  $s$  that satisfies  $X(t, t, \xi) = \xi$ , where in general  $\xi = (\mathbf{x}, \mathbf{v})$ . For the rest of this section, we restrict the calculations to one dimension. The generalisation to the higher dimensional system will be given later. We thus assume  $\xi \in \mathbb{R}$ . Then we can integrate (26) and obtain a propagator from time  $t^n$  to time  $t^{n+1}$

$$\int_{x_{i-1/2}}^{x_{i+1/2}} f(x, t^{n+1}) dx = \int_{X(t^n, t^{n+1}, x_{i-1/2})}^{X(t^n, t^{n+1}, x_{i+1/2})} f(x, t^n) dx. \quad (27)$$

Here  $x_{i-1/2}$  and  $x_{i+1/2}$  are the boundaries of the numerical grid cell  $i$ . The discretisation of the distribution function is now suggested by the above equation. The values  $f_i^n$  on the numerical grid represent the cell integrals

$$f_i^n = \frac{1}{\Delta x} \int_{x_{i-1/2}}^{x_{i+1/2}} f(x, t^n) dx.$$

We also define the flux through a cell boundary at  $x_{i+1/2}$  during the time interval  $[t^n; t^{n+1}]$

$$\Phi_{i+1/2}^n = \int_{X(t^n, t^{n+1}, x_{i+1/2})}^{x_{i+1/2}} f(x, t^n) dx$$

Then equation (27) can be expressed in the following form

$$f_i^{n+1} = \Phi_{i-1/2}^n + f_i^n - \Phi_{i+1/2}^n. \quad (28)$$

This equation still follows exactly from Vlasov's equation. However, the flux  $\Phi$  has to be calculated, and this requires an approximation of the distribution function.

In the framework of the third order positive and flux conservative scheme, as presented by [23], the primitive of the distribution function is approximated using a four point stencil. Let

$$F(x, t^n) = \int_{x_0}^x f(x', t^n) dx', \quad (29)$$

then it follows exactly that

$$F(x_{i+1/2}, t^n) = \Delta x \sum_{k=0}^i f_k^n \equiv F_i^n. \quad (30)$$

The primitive is given exactly on the cell boundaries. To approximate  $F(x, t^n)$  in the cell interval  $[x_{i-1/2}; x_{i+1/2}]$ , the four points  $\{x_{i-3/2}, x_{i-1/2}, x_{i+1/2}, x_{i+3/2}\}$  are used. Taking the derivative of the primitive, we recover the approximation of the distribution function

$$\begin{aligned} f_{\approx}(x) = & f_i + \frac{\epsilon_i^+}{6\Delta x^2} \left[ 2(x - x_i)(x - x_{i-3/2}) \right. \\ & \left. + (x - x_{i-1/2})(x - x_{i+1/2}) \right] (f_{i+1} - f_i) \\ & - \frac{\epsilon_i^-}{6\Delta x^2} \left[ 2(x - x_i)(x - x_{i+3/2}) \right. \\ & \left. + (x - x_{i-1/2})(x - x_{i+1/2}) \right] (f_i - f_{i-1}). \end{aligned} \quad (31)$$

Here limiters  $\epsilon_i^{\pm}$  are introduced. The limiters are chosen in such a way as to limit the values of the distribution function to a fixed interval  $0 \leq f_{\approx}(x) \leq f_{\infty}$ , where  $f_{\infty}$  is the maximum of all  $f_i$ . The  $\epsilon_i^{\pm}$  can be written as

$$\epsilon_i^+ = \begin{cases} \min(1; 2f_i/(f_{i+1} - f_i)) & \text{if } f_{i+1} - f_i > 0 \\ \min(1; 2(f_{\infty} - f_i)/(f_i - f_{i+1})) & \text{if } f_{i+1} - f_i < 0 \end{cases} \quad (32)$$

and

$$\epsilon_i^- = \begin{cases} \min(1; 2(f_{\infty} - f_i)/(f_i - f_{i-1})) & \text{if } f_i - f_{i-1} > 0 \\ \min(1; 2f_i/(f_{i-1} - f_i)) & \text{if } f_i - f_{i-1} < 0 \end{cases}. \quad (33)$$

If we determine  $j$  such that  $x_{j-1/2} \leq X(t^n, t^{n+1}, x_{i+1/2}) < x_{j+1/2}$ , we get

$$\begin{aligned} \Phi_{i+1/2} = & (1 - \delta) \left[ f_j + (1/6)\delta(\delta + 1)\epsilon^+(f_{j+1} - f_j) \right. \\ & \left. - (1/6)\delta(\delta - 2)\epsilon^-(f_j - f_{j-1}) \right] + \Delta x \sum_{k=\min(i,j)+1}^{\max(i,j)-1} f_k, \end{aligned} \quad (34)$$

where  $\delta = X(t^n, t^{n+1}, x_{i+1/2}) - x_{j-1/2}$ .

## 5 Time splitting and integration of characteristics

The above scheme was presented in one dimension. To perform two dimensional Vlasov-simulations including magnetic fields, the scheme has to be generalised to a total of 5 dimensions. Califano et al. [28] proposed a scheme in which the individual steps for the different dimension are carried out using a

second order time splitting scheme. The scheme is an extension of the time splitting scheme presented by Cheng and Knorr [29]. For the two spatial directions  $x$  and  $y$ , the projection of the characteristics onto the axes is simply evaluated from by the corresponding velocity components  $v_x$  and  $v_y$ . In this way, the two space dimensions are independent of each other and can be performed sequentially,

$$T_{\mathbf{x}} = T_x T_y \quad (35)$$

where  $T_k$  denotes a time-integration step in one dimension with the direction  $k$ . In contrast to this, the velocity components are not independent of each other due to the magnetic field. To create a second order scheme Califano et al. [28] formulated a straightforward second order time splitting scheme,

$$T_{\mathbf{v}}(\Delta t) = T_{vx}\left(\frac{\Delta t}{4}\right)T_{vy}\left(\frac{\Delta t}{2}\right)T_{vx}\left(\frac{\Delta t}{4}\right)T_{vz}(\Delta t)T_{vx}\left(\frac{\Delta t}{4}\right)T_{vy}\left(\frac{\Delta t}{2}\right)T_{vx}\left(\frac{\Delta t}{4}\right). \quad (36)$$

This propagator in the velocity directions was then combined with the propagator in the space directions to create the full scheme,

$$T_{\text{full}}(\Delta t) = T_{\mathbf{x}}(\Delta t/2)T_{\mathbf{v}}(\Delta t)T_{\mathbf{x}}(\Delta t/2). \quad (37)$$

In the following we will refer to this method as the *time splitting* method.

We implemented and tested this scheme, but found it to suffer from substantial inaccuracies, as shown in section 6.1. Therefore, a new scheme for the integration is proposed in this work which we call the back substitution method. Here, the integration of Vlasov's equation in the three velocity dimensions is still split into three separate steps, one for each direction. The difference to the above scheme is the way the integration of the characteristics is separated out into the three substeps. This implies that the concrete implementation of the scheme proposed here depends on the method of integration of the characteristics. We will therefore quickly present Boris' scheme for integration of characteristics in a magnetic field [27,30,31]. Boris' scheme is widely used in Particle codes and has the advantage that it is a second order integration scheme in which the magnetic field does not cause a change in the kinetic energy. The integration step is formulated as an implicit finite difference scheme

$$\frac{\mathbf{v}^{n+1} - \mathbf{v}^n}{\Delta t} = \frac{q}{m} \left( \mathbf{E} + \frac{\mathbf{v}^{n+1} + \mathbf{v}^n}{2} \times \mathbf{B}. \right) \quad (38)$$

The electric and magnetic forces are separated,

$$\mathbf{v}^- = \mathbf{v}^n + \frac{\Delta t}{2} \frac{q}{m} \mathbf{E}, \quad (39)$$

$$\mathbf{v}^+ = \mathbf{v}^{n+1} - \frac{\Delta t}{2} \frac{q}{m} \mathbf{E}, \quad (40)$$

leading to

$$\frac{\mathbf{v}^+ - \mathbf{v}^-}{\Delta t} = \frac{q}{2m} (\mathbf{v}^+ + \mathbf{v}^-) \times \mathbf{B}. \quad (41)$$

The transformation from  $\mathbf{v}^-$  to  $\mathbf{v}^+$  is a pure rotation with an angle  $\theta$ , where

$$\left| \tan \frac{\theta}{2} \right| = \frac{\Delta t q B}{2 m}. \quad (42)$$

To implement this rotation the vectors  $\mathbf{t}$  and  $\mathbf{s}$  are defined

$$\mathbf{t} = \frac{\Delta t q \mathbf{B}}{2 m}, \quad \mathbf{s} = \frac{2\mathbf{t}}{1 + t^2}. \quad (43)$$

Then the rotation is performed in two steps

$$\mathbf{v}' = \mathbf{v}^- + \mathbf{v}^- \times \mathbf{t} \quad (44)$$

and

$$\mathbf{v}^+ = \mathbf{v}^- + \mathbf{v}' \times \mathbf{s}. \quad (45)$$

This scheme supplies  $\mathbf{v}^{n+1} = (v_x^{n+1}, v_y^{n+1}, v_z^{n+1})$  in terms of  $\mathbf{v}^n = (v_x^n, v_y^n, v_z^n)$ .

For the integration of Vlasov's equation in three dimensional velocity space the three individual integration steps are performed in turn, thus, the integration of the characteristics also has to be split into three separate steps. For this, two things have to be considered. Firstly, when integrating one component of the velocity, we take into account the shifts of the distribution function that have already been performed. Secondly, we then have to observe the order of integration, which is reversed with respect to the integration of a particle trajectory. This follows from the fact that, for the Vlasov scheme, the characteristics have to be traced backwards in time.

For clarity, we will present the back substitution method for forward integration of the characteristics. Later, we will reverse the order of the substeps for the backward integration needed in the Vlasov scheme. For forward integration, first, the integration in  $v_x$  is performed, as described in the discussion of Boris' scheme above. For the integration of the characteristics this means  $v_x^{n+1} = v_x^{n+1}(v_x^n, v_y^n, v_z^n)$ . When the integration along the  $v_y$ -direction is performed, in the next step, the shift along the  $v_x$ -direction has already been performed. For the integration of the characteristics this means that a scheme calculating  $v_y^{n+1} = v_y^{n+1}(v_x^{n+1}, v_y^n, v_z^n)$  is needed. In the above notation, it is sufficient to reformulate the integration to give  $v_y^+ = v_y^+(v_x^+, v_y^-, v_z^-)$ . This can be achieved using simple algebraic manipulations and eliminating  $v_x^-$ . For the last integration step along the  $v_z$ -direction, one can find in the same manner a scheme giving  $v_z^+ = v_z^+(v_x^+, v_y^+, v_z^-)$ . The details of this scheme are presented in appendix A. The scheme has also been implemented and it was found to be less diffusive than the second order time splitting scheme (see section 6.1). As stated above, the characteristics have to be traced backwards in time. To this end, we reverse the order of integration, without changing the above formulas; i.e. we first shift the distribution function in the  $v_z$ -direction using

$v_z^+ = v_z^+(v_x^+, v_y^+, v_z^-)$ , then in the  $v_y$ -direction using  $v_y^+ = v_y^+(v_x^+, v_y^-, v_z^-)$ , and finally in the  $v_x$ -direction using  $v_x^{n+1} = v_x^{n+1}(v_x^n, v_y^n, v_z^n)$ .

The splitting of the integration into individual steps introduces another problem, independent of the splitting scheme used. The limiters  $\epsilon_i^+$  and  $\epsilon_i^-$  guarantee only that the distribution function is positive and limited by  $f_\infty$  from above for incompressible transport equations. The Vlasov equation together with any set of equations for the electromagnetic fields presents such a system. Due to the separation of the integration along the different directions in velocity space together with the forces originating from the magnetic field, the single integration steps are, however, not incompressible. This holds for both the splitting and the back substitution scheme. The first direction of integration might compress the distribution function in the  $v_x$  direction, while the successive integrations decompress the distribution function in the  $v_y$  and  $v_z$  directions. In the end the total compression will always vanish. The maximum value of the distribution function might however increase during an intermediate step.

We present two types of calculations. In the first we omit the limiter from above completely, allowing the distribution function to rise uncontrollably. The limiters  $\epsilon_i^+$  and  $\epsilon_i^-$  are then given by

$$\epsilon_i^+ = \begin{cases} \min(1; 2f_i/(f_{i+1} - f_i)) & \text{if } f_{i+1} - f_i > 0 \\ 1 & \text{if } f_{i+1} - f_i < 0 \end{cases} \quad (46)$$

and

$$\epsilon_i^- = \begin{cases} 1 & \text{if } f_i - f_{i-1} > 0 \\ \min(1; 2f_i/(f_{i-1} - f_i)) & \text{if } f_i - f_{i-1} < 0 \end{cases}. \quad (47)$$

This means, the maximum principle, that was fulfilled by the original scheme, is now no longer satisfied. In the second type of simulation we keep the original limiters (32) and (33) but determine  $f_\infty$  to be the global maximum of the distribution function after each intermediate integration step for each direction in velocity space.

## 6 Numerical tests

The third order positive flux conservative method has been extensively tested in one dimension and in the electrostatic limit [23]. Here, we first want to present results of the integration scheme in three dimensional velocity space with a given magnetic field. We compare the results of the two integration schemes and a standard second order finite difference scheme. The latter is included in the comparison since it has been used for Vlasov simulations of reconnection by various authors.

In the second part of this section we present results of reconnection simulations. These have been carried out using both the flux conservative scheme with the back substitution method and the finite difference scheme. Results of the two are compared.

### 6.1 Gyro motion

To test the quality of the Vlasov integration scheme together with the integration of the characteristics a simple test system was simulated. In this test only one positively charged species was simulated in a constant magnetic field  $\mathbf{B} = B_0 \mathbf{e}_z$ , with  $B_0 = 1$ . The initial distribution function was taken to be a shifted Maxwellian

$$f(\mathbf{x}, \mathbf{v}) = \exp \left[ -(\mathbf{v} - \mathbf{v}_0)^2 \right], \quad (48)$$

where  $\mathbf{v}_0 = v_0 \mathbf{e}_x$  is a constant velocity in the  $x$ -direction. There was no spatial variation, and so a simple gyro motion of the thermal peak in velocity space is expected. However, due to numerical errors this peak will change its shape. These numerical errors only appear in the presence of a magnetic field. In the pure one dimensional advection problem only small errors compared with the exact solution are found.

We have simulated the gyro motion of a thermal peak using the two different integration methods for the characteristics, different time steps, and varying resolutions of the grid in the velocity dimensions. Additional simulations have been carried out using a simple finite difference scheme. The scheme is obtained from eq (2) by substituting all partial derivatives by their centred finite difference approximation over one grid cell. A third order Runge-Kutta method is used for the time step. In Figure 1 the  $v_x$ - $v_y$  distribution function is shown for the case of  $N_v = 30$  and  $\Delta t = 2\pi\Omega_c/200$  using the flux conservative scheme with the back substitution algorithm for integration of the characteristics. The  $z$ -scaling is arbitrary but identical in the three sub-plots of Figure 1. Initially (a), the distribution function is set to the shifted Maxwellian. At  $t = 2\pi\Omega_c$  (b), the peak has performed one full gyration. A slight dissipation can be observed. The dissipation has increased after five gyration periods  $t = 10\pi\Omega_c$  (c). With the above time step, this correspond to a total of 1000 time steps.

The dissipation in phase space can be quantified by taking the second moment of the distribution function  $\langle (v - \langle v \rangle)^2 \rangle = \langle v^2 \rangle - \langle v \rangle^2$  which represents the thermal energy in the system. These have been calculated over a time of five gyro-periods for different simulation time steps, different grid resolutions of the phase space, and different time splitting algorithms. In Figure 2 the thermal energies are shown for both the back-substitution algorithm (upper panel) and for the time splitting algorithm (lower panel), both taken without

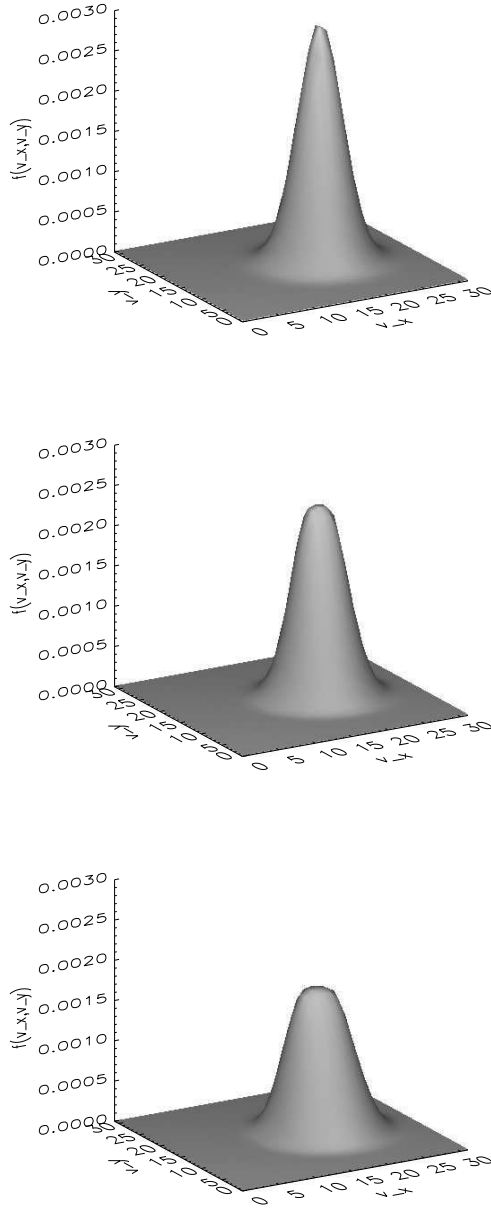


Fig. 1. Gyration of a Maxwellian peak using the back-substitution algorithm with  $N_v = 30$  and  $\Delta t = 2\pi\Omega_c/200$  (a) initially, (b) after one gyration period and (c) after five gyration periods. The scale on the  $z$ -axis is in arbitrary units but identical in the three diagrams.

limiting the distribution function from above. For a small time step  $\Delta t = 0.01\Omega_c/\pi$ , i.e. a time-resolution of 200 time steps per gyration, calculations using  $N_v = 10$  and  $N_v = 30$  grid points per velocity dimension have been carried out. In the case of  $N_v = 10$  and using the back-substitution algorithm, the thermal energy rises more than a factor of 4.5 during the simulated time period. The amount of diffusion can be reduced considerably by increasing the

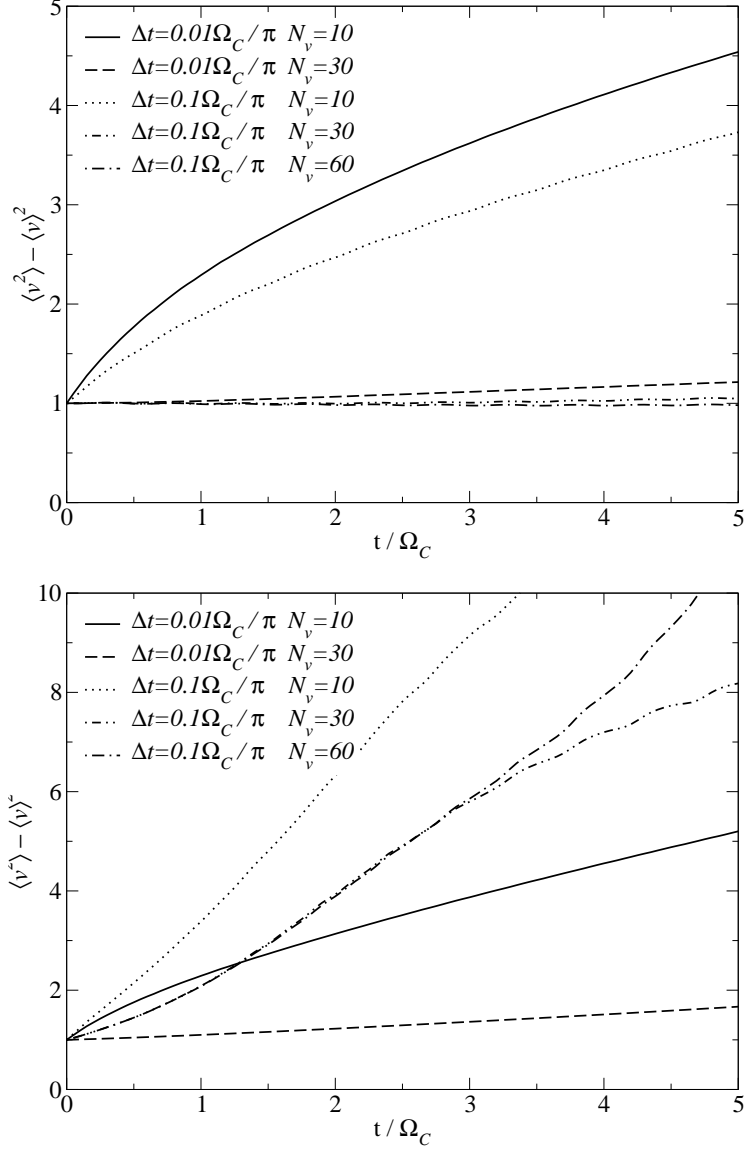


Fig. 2. The thermal energy of the distribution function  $\langle v^2 \rangle - \langle v \rangle^2$  during five gyro-periods for different time-steps and different phase space resolutions. The upper panel shows the curves resulting from the back-substitution algorithm, the lower panel those resulting from the time splitting algorithm. No limiting from above was applied

grid resolution. At  $N_v = 30$ , the increase in thermal energy reduces to around 20% over the simulated five gyro-periods.

For  $N_v = 10$ , an increase in the time step by a factor of 10 does not modify the results by a great amount. The already large diffusion values remain similar although somewhat lower. In contrast, for the  $N_v = 30$  case, the thermal energy at the end of the simulation is risen only by less than 5% from the starting value, for a time step of  $\Delta t = 0.1\Omega_c/\pi$ , i.e. 20 time steps per gyration.



This means that an increase in the time steps leads to better results for the thermal energy. An increase in grid resolution further improves the result and reduces the error to less than 2%.

The results using the time splitting scheme (lower panel of Figure 2) differ considerably from the previous results. Again, the thermal energy in the small time step case with  $N_v = 10$  rises strongly. This now gets substantially less accurate by increasing the time step to 20 steps per gyration. Here, the thermal energy increases by more than a factor of 12! The best result is achieved by taking a small time step and a grid resolution of  $N_v = 30$ . Instead of a slight increase in thermal energy, a slight decrease can be observed here. Increasing the time step to 20 steps per gyration degrades the results again. A strong increase in the thermal energy is observed, which is even *worse* for *higher* grid resolutions.

In Figure 3 the same results are shown again, but this time with the limiting from above switched on. These results differ only marginally from those obtained without the limiter in place. Note, that the limiter ensuring positivity of the distribution function is always in place. Summarising, one finds that the back-substitution method gives superior results over the time-splitting method. Furthermore in terms of thermal energy, the back-substitution method rewards larger time steps (i.e. less computational time) with higher accuracy.

Instead of looking at the thermal energy, which is related to dissipation in phase space, one can also investigate the gyro-motion of the Maxwellian peak. From the distribution function the averages  $\langle v_x \rangle$  and  $\langle v_y \rangle$  are taken and plotted against each other through time. In the exact case, this should result in perfectly circular motion with exactly one turn during a gyration period  $2\pi/\Omega_C$ . The numerical Vlasov scheme does not, however, produce exact results and thus one will observe some form of spiral. An example of this spiral is plotted in Figure 4.

After some time one can observe errors in both the absolute magnitude of the velocity and in the phase of the gyro-motion. For the same parameters as above, the magnitude of the velocity after five gyro-periods is given in table 1, for the various schemes and numerical parameters. Table 2 shows the corresponding phase errors in radians.

The back-substitution shows better results both for the large and the small time steps than the time splitting method. The best overall result is achieved by the back-substitution method in conjunction with a small time step and a grid resolution of  $N_v = 30$ . Only a marginal phase error can be observed. There is almost no error in the average velocity. A decrease of the grid resolution

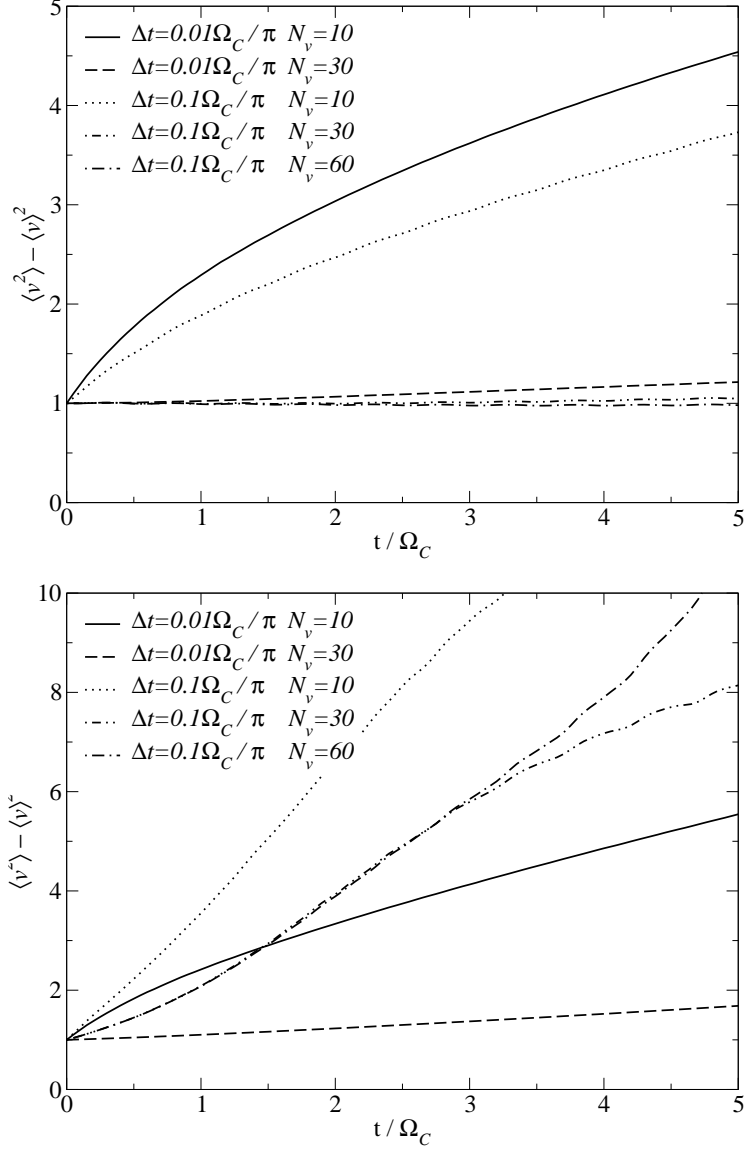


Fig. 3. The thermal energy of the distribution function  $\langle v^2 \rangle - \langle v \rangle^2$  during five gyro-periods for different time-steps and different phase space resolutions. The upper panel shows the curves resulting from the back-substitution algorithm, the lower panel those resulting from the time splitting algorithm. Limiting from above was applied

results in a positive phase error and a decrease of the velocity magnitude error. In contrast, an increase of the time step causes a rise in the velocity magnitude together with an increase of the phase error. Here now, an increase in the grid resolution from 30 to 60 does not improve the results when using a large time step. For a resolution of 10 and a large time step only the phase error increases. One can note, that in all these cases the phase error is negative. This means that the simulated gyro motion always lags behind the physical gyro motion.

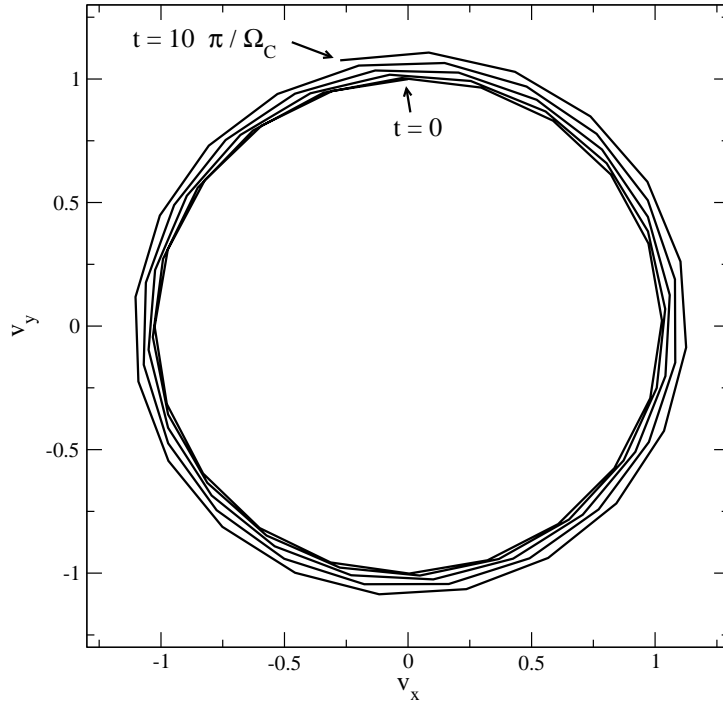


Fig. 4. The gyro-motion of the Maxwellian peak expressed in  $\langle v_y \rangle$  against  $\langle v_x \rangle$  over five gyro-periods. After five gyro-periods the mean velocity has an error in magnitude and phase from the starting value.

$\Delta t$	$N_v$	Back Substitution		Splitting		Finite Diff.	
		limiter	no limiter	limiter	no limiter	2nd order	4th order
$\pi/100$	10	0.8892	0.9178	1.0843	1.0496	1.09933	1.04747
$\pi/100$	30	0.9981	0.9991	1.2029	1.2021	0.998163	0.999867
$\pi/10$	10	1.1100	1.1082	2.1824	2.0992	unstable	unstable
$\pi/10$	30	1.1301	1.1328	2.9553	2.9452	unstable	unstable
$\pi/10$	60	1.1190	1.1209	4.0757	4.0402	unstable	unstable

Table 1

Magnitude of the Maxwellian peak after five gyro-periods for different time-steps, different phase space resolutions and different integration methods. The magnitudes are normalised to the initial height of the peak.

The errors in phase and velocity magnitude are generally larger when using the time splitting method. With the large time step the magnitude of the velocity goes up by approximately 2 to 4 times the initial velocity. The velocity error is lower when using the small time step; however, for the high resolution the error is still 20%. Only the low resolution, large time step case has a relatively small error in the magnitude. This is accompanied by a large error in phase. For resolutions 30 and 60 the phase error is better than the one found with

$\Delta t$	$N_v$	Back Substitution		Splitting		Finite Diff.	
		limiter	no limiter	limiter	no limiter	2nd order	4th order
$\pi/100$	10	0.04214	0.06544	0.1512	0.1363	2.05693	1.99755
$\pi/100$	30	-0.04178	-0.03969	-0.01143	-0.01341	2.07876	2.10456
$\pi/10$	10	-0.2500	-0.2349	0.6331	0.6002	unstable	unstable
$\pi/10$	30	-0.08965	-0.09051	0.09543	0.08768	unstable	unstable
$\pi/10$	60	-0.09232	-0.09244	0.05441	0.05011	unstable	unstable

Table 2

Phase error of the Maxwellian peak after five gyro-periods for different time-steps, different phase space resolutions and different integration methods.

the back-substitution method. The error in the velocity magnitude here is on the other hand, unacceptable. In both cases one finds that switching on the limiter does not modify any of these results considerably.

Finally, comparing this with the results from the finite difference scheme one finds that the flux conservative approach is far superior in all cases. Although the finite difference schemes show small amplitude errors, phase errors are serious. In addition, for the large time steps the finite difference scheme becomes completely unstable (in agreement with the CFL condition).

## 6.2 Reconnection

A test of the complete Vlasov–Darwin system has been performed on a magnetic reconnection setup, including full ion and electron dynamics. As pointed out in the introduction, research on magnetic reconnection is still one of the most challenging topics in collisionless plasmas. Kinetic simulations using a Vlasov code have been carried out, for example by Silin and Büchner [18]. Since these simulations were carried out using a finite difference scheme, we will here again present the results of both finite difference and the flux conservative scheme. We used a simulation box consisting of  $50 \times 100$  grid cells in space with a grid spacing of  $\Delta x = 0.1$ . The total size of the simulation box is  $L_x = 10$  by  $L_y = 5$ . There are  $10 \times 10 \times 10$  grid cells in velocity space. Although the resolution in velocity space is — as shown above — insufficient for the gyro motion, especially for the finite difference scheme, this low resolution is chosen for a number of reasons. Firstly, it keeps the computational effort to a reasonable magnitude. Secondly, this corresponds to the phase space resolution chosen by Wiegmann and Büchner [19] and thus allows some comparison. Thirdly, we think that the pure gyro motion test is a very strict test for the numerical scheme. In the most regions of the reconnection simulation, the magnetic field is balanced by some electric field or by the density gradient in such a way that

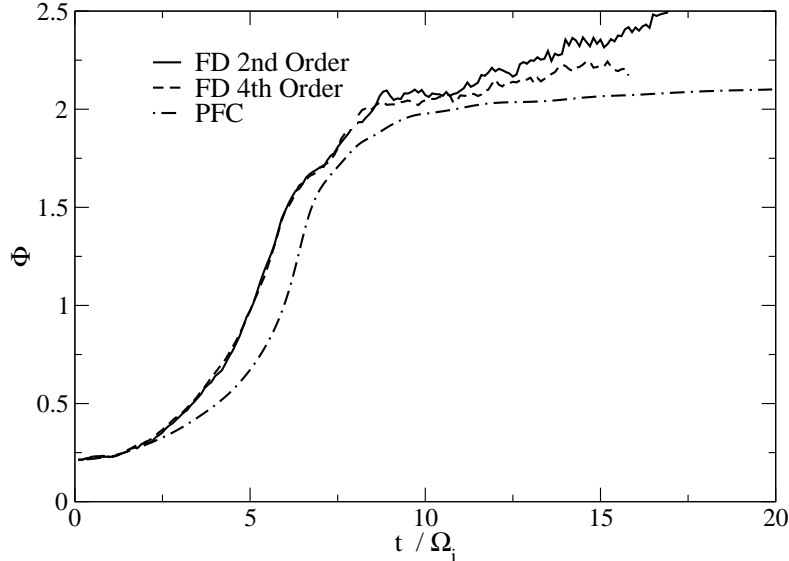


Fig. 5. The reconnected magnetic flux  $\Phi$  over time. The solid line is the result of the second order finite difference scheme. The dashed line is the result of a fourth order finite difference scheme. The dashed-dotted line is the result from the flux conservative scheme.

the gyro motion does not occur the way as presented in the previous section. The mass ratio between electrons and ions has been chosen to  $m_i/m_e = 16$  and the time step is

$$\Delta t = 2.5 \cdot 10^{-3} = \frac{1}{25\Omega_{ce}}, \quad (49)$$

where  $\Omega_{ce}$  is the electron Larmor frequency in the unit magnetic field. Simulations with half this time step have been performed as convergence test (not shown here) but no substantial deviations have been found.

The initial conditions are chosen as two opposite current sheets. Each current layer has the well known Harris sheet profile [1] together with a small perturbation. The distribution function is given by a shifted Maxwellian

$$f_{i,e}(x, y) = \rho(x, y) \exp\left(\frac{m_j}{2kT_j} (v_x^2 + v_y^2 + (v_z - v_0^\pm)^2)\right), \quad (50)$$

with  $v_0^\pm = \pm 1$ . The particle density  $\rho(x, y)$  is given by

$$\rho(x, y) = \frac{1}{\cosh\left(\frac{y - y_0^\pm}{\lambda}\right)} \left(1 + \varepsilon \cos\left(\frac{2\pi(x - x_0^\pm)}{L_x}\right)\right). \quad (51)$$

The two Harris sheets, positioned at  $y^+ = L_y/4$  and  $y^- = 3L_y/4$ , carry opposite current, and the perturbations have a relative shift along the  $x$ -axis

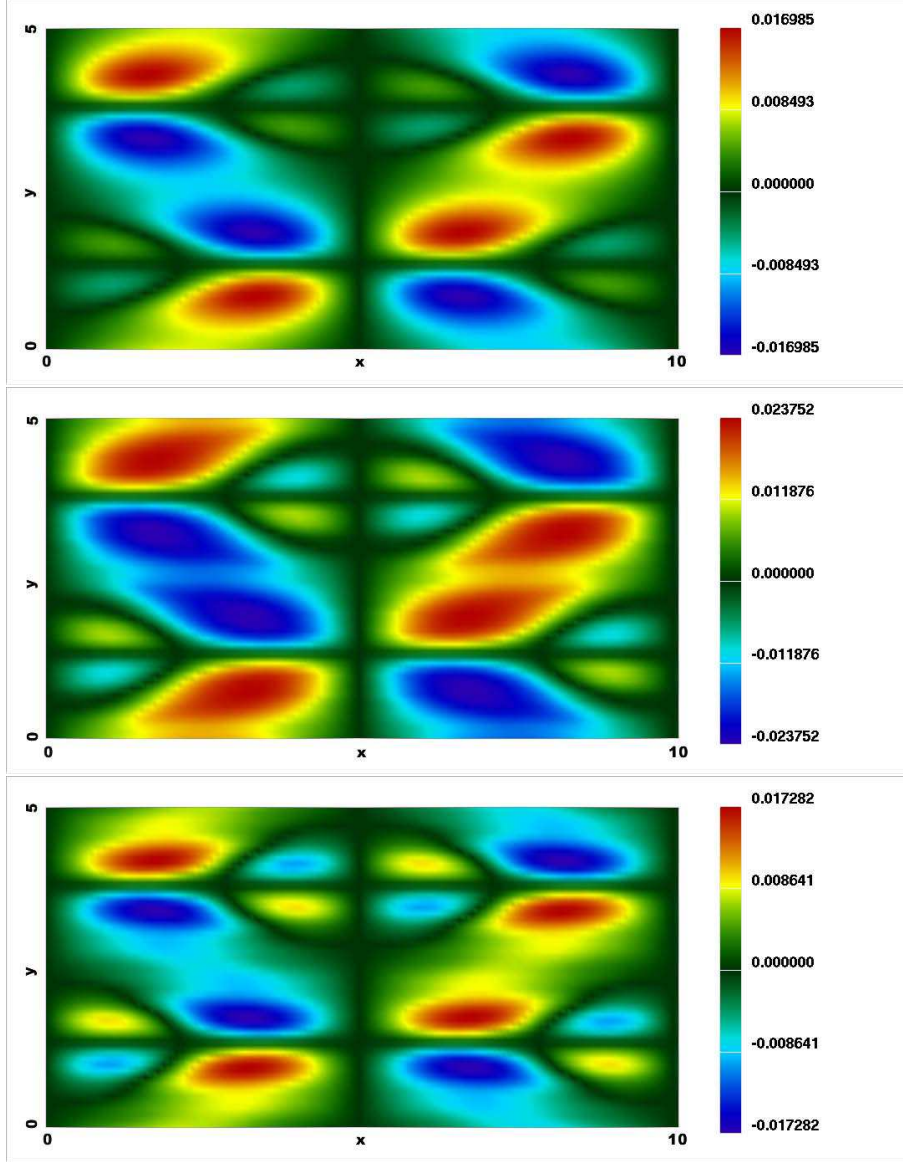


Fig. 6. The out of plane magnetic field component  $B_z$  in the simulation box at  $t = 4.1$  using the back-substitution method (upper panel) and at  $t = 3.1$  using the finite difference scheme in 2nd order (middle panel) and 4th order (lower panel).

of  $\pi/L_x$ , given by  $x^+ = 0$  and  $x^- = 1/2$ . The perturbation has a value of  $\varepsilon = 0.05$ . Periodic boundary conditions are used both in the  $x$  and  $y$  direction. The X-points will then develop at  $X^+ = (5, 1.25)$  and  $X^- = (0, 3.75)$ .

Figure 5 shows the temporal evolution of the reconnected flux. The curves are quite similar keeping in mind that the resolution is marginal. The major difference is the slightly earlier onset of reconnection for the finite difference runs.

If one wants to compare the schemes, one has to choose the time for the different simulations separately such that the reconnected flux is the same for all

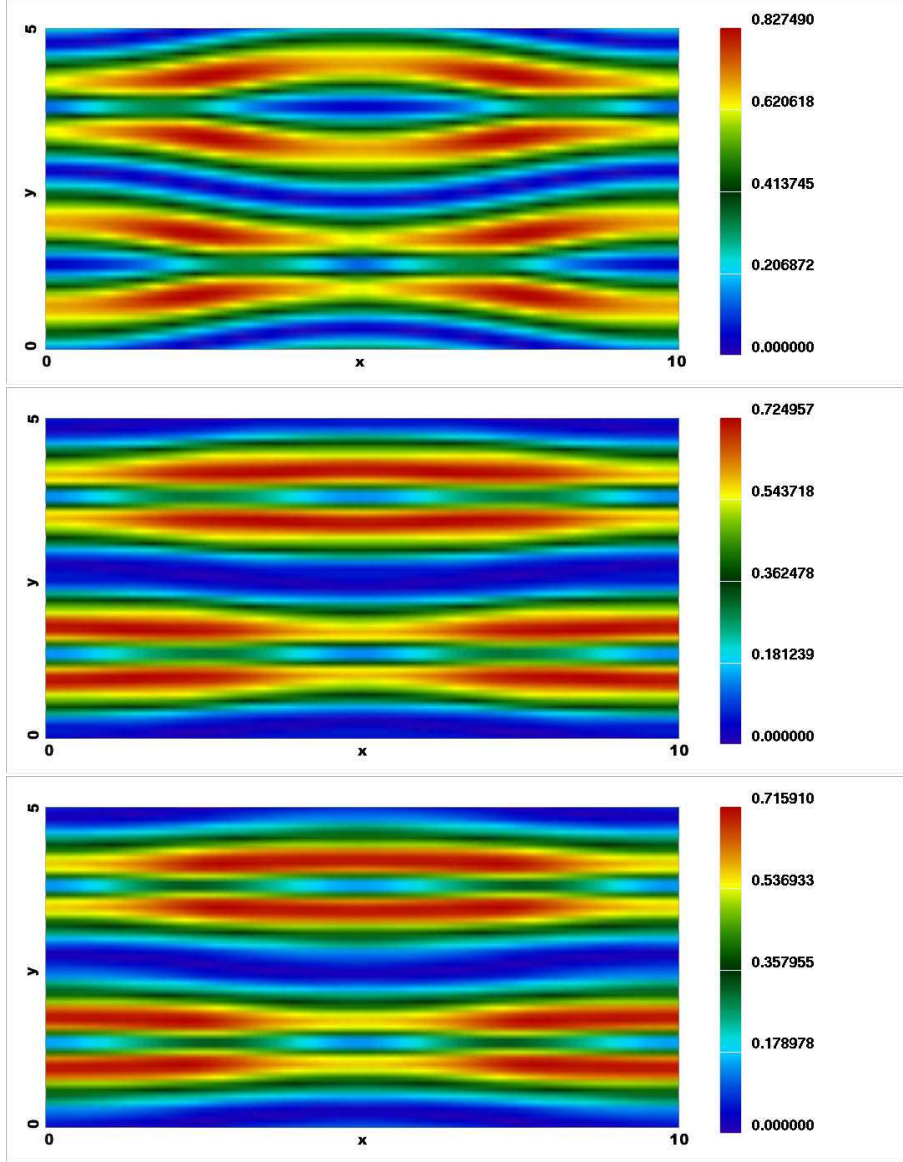


Fig. 7. The magnitude of the Hall term  $|(\mathbf{j} \times \mathbf{B})_z|$  in the simulation box at  $t = 4.1$  using the back-substitution method (upper panel) and at  $t = 3.1$  using the finite difference scheme in 2nd order (middle panel) and 4th order (lower panel).

simulations. Therefore, we choose a time at the beginning of the reconnection phase which corresponds to  $t = 4.1$  for the flux conservative method and to  $t = 3.1$  for the finite difference schemes.

Figure 6 shows the perpendicular magnetic field  $B_z$ . The upper panel shows the result of the flux conservative simulation while the mid and lower panel display the results of the finite difference schemes (mid: second order, lower: fourth order). One can clearly see the quadrupolar structure of the magnetic field component at the X-point which has been observed in previous simulations of the reconnection process. There is a slight difference in the distribution of the

magnetic field component between the simulations. One significant difference is the magnitude of  $B_z$ . The values are considerably larger in the second order finite difference scheme than in the flux conservative scheme and fourth order finite difference scheme.

In Figure 7 the magnitude of the  $z$ -component of the Hall-term  $|(\mathbf{j} \times \mathbf{B})_z|$  is shown for the different schemes. This quantity can be taken as a measure for the importance of the Hall term when comparing to MHD models. All simulations show qualitatively a similar behaviour. From the results of the flux conservative simulation one can see that the  $z$ -component of the Hall term is largest outside of the X-points.<sup>1</sup>

## 7 Conclusions

A 5 dimensional Vlasov code using the Darwin approximation of Maxwell's equations has been presented. While in the past a lot of development has gone into developing numerical schemes for one dimensional electrostatic Vlasov codes, there is a growing need for kinetic codes that include the effects of the magnetic field. This is needed for both the simulation of astrophysical as well as laboratory plasmas. For a large number of problems the electromagnetic vacuum modes contained in the full set of Maxwell equations is not of major importance for the physical processes. These, however, pose severe restrictions on the simulation parameters, due to the CFL criterion. The Darwin approximation resolves this problem by eliminating the vacuum modes without reverting to the electrostatic limit. In contrast to other approximation of Maxwell's equations, the Darwin approximation can be shown to consistently emerge from an expansion of the full equations in orders of  $v_0^2/c^2$ . The Darwin approximation has been used extensively in particle in cell simulations but has not found it's way into Vlasov codes until now. Within the framework of the Darwin approximation the purely electromagnetic modes are cancelled, but the modes that rely on the plasma reaction to the magnetic field are retained, such as the magnetosonic or Alfvén modes.

For the integration of the Vlasov equation in time a recently developed flux conservative scheme [23] has been used. The scheme, which was originally proposed for a one dimensional electrostatic system had, to be generalised for the higher dimensional phase space required for the Vlasov–Darwin system. The generalisation of the one dimensional system is ambiguous and two different schemes have been compared: the straightforward time splitting scheme [28] using a generalised time splitting iteration was shown to suffer from substantial inaccuracies; the back substitution scheme, proposed in this work, gives far better results not only in terms of an accurate reproduction of the gyro motion but also concerning the controllability of the errors. Results were also



compared to finite difference simulations which were shown to be greatly inaccurate in comparison to the flux conservative scheme.

Finally, a simulation of magnetic reconnection has been performed to test the full Vlasov–Darwin system. For comparison, the same system has also been simulated using the finite difference scheme. The finite difference scheme has been chosen as a reference scheme since this is the most common approach for simulation magnetic reconnection using a Vlasov code. Substantial improvements were achieved using the code presented here. The results especially of derived quantities, did not suffer from numerical fine scale distortions. It was shown that the results of the scheme presented here can be treated as much more reliable than those of a finite difference scheme.

The code presented here may be used for the investigation of magnetic reconnection processes and for the simulation of nonrelativistic collisionless shocks. The main advantages, as compared to PIC simulations, is the absence of numerical noise and the access to the full distribution function, especially the high energy tails. In PIC simulations these high energy tails generally suffer from bad statistics. For this reason it might be of interest to use Vlasov codes to simulate particle acceleration.

One should note however that, because of the large computational time, the applicability of Vlasov codes at this time stays restricted to two dimensional models. Again, in comparison to PIC codes, Vlasov codes are slower by a factor of a hundred. Despite this comparatively large numerical effort, Vlasov simulations are still valuable since they complement other simulation techniques.

## Acknowledgements

We acknowledge interesting discussions with J. Büchner, J. Dreher and R. Sydora. This work was supported by the SFB 591 of the Deutsche Forschungsgesellschaft. Access to the JUMP multiprocessor computer at Forschungszentrum Jülich was made available through project HBO20.

## A Back–Substitution Method for Integration of Characteristics

Here we present the formulae for the integration of the characteristics in the velocity space using the back–substitution method. The three integrations in  $v_x$ ,  $v_y$  and  $v_z$ –direction are carried out individually. The underlying equations have been presented in section 5 but are in an implicit form for our purpose.

Here we want to give explicit formulae for the three steps

$$v_x^{n+1} = v_x^{n+1}(v_x^n, v_y^n, v_z^n), \quad (\text{A.1})$$

$$v_y^{n+1} = v_y^{n+1}(v_x^{n+1}, v_y^n, v_z^n), \quad (\text{A.2})$$

$$v_z^{n+1} = v_z^{n+1}(v_x^{n+1}, v_y^{n+1}, v_z^n). \quad (\text{A.3})$$

Since the bijections between  $v^n$  and  $v^-$  on one hand and  $v^{n+1}$  and  $v^+$  on the other hand are trivial (see eqs (39) and (40)) it is sufficient to formulate the three steps

$$v_x^+ = v_x^+(v_x^-, v_y^-, v_z^-), \quad (\text{A.4})$$

$$v_y^+ = v_y^+(v_x^+, v_y^-, v_z^-), \quad (\text{A.5})$$

$$v_z^+ = v_z^+(v_x^+, v_y^+, v_z^-). \quad (\text{A.6})$$

By virtue of equations (44) and the  $x$ -component of (45),  $v_x$  is already given in the above form. The integration in  $v_x$  is identical to the integration used in the time splitting algorithm.

In the second integration step  $v_y^+$  has to be determined from  $(v_x^+, v_y^-, v_z^-)$ . The  $y$ -component of equation (45) gives  $v_y^+ = v_y^+(v_x^-, v_y^-, v_z^-)$ . However, the  $x$ -component of that equation can now be solved for  $v_x^-$  to give

$$v_x^- = v_x^-(v_x^+, v_y^-, v_z^-) = \frac{1}{A_x} \left( v_x^+ - v_y^-(s_z + s_y t_x) - v_z^-(s_y - s_z t_x) \right), \quad (\text{A.7})$$

with

$$A_x = 1 - s_y t_y - s_z t_z \quad (\text{A.8})$$

With this we get

$$v_y^+(v_x^+, v_y^-, v_z^-) = v_y^+(v_x^-(v_x^+, v_y^-, v_z^-), v_y^-, v_z^-). \quad (\text{A.9})$$

In the same manner the  $z$ -component of equation (45) gives  $v_z^+ = v_z^+(v_x^-, v_y^-, v_z^-)$ . Then the  $x$  and the  $y$ -components of that equation are used to solve for  $v_x^-$  and  $v_y^-$

$$v_x^- = \frac{(1 - s_x t_x - s_z t_z)(v_x^+ + (s_y - s_z t_x)v_z^-) - (s_z + s_y t_x)(v_y^+ - (s_x + s_z t_y)v_z^-)}{(1 - s_y t_y - s_z t_z)(1 - s_x t_x - s_z t_z) + (s_z + s_y t_x)(s_z - s_x t_y)}, \quad (\text{A.10})$$

$$v_y^- = \frac{(s_z - s_x t_y)(v_x^+ + (s_y - s_z t_x)v_z^-) + (1 - s_y t_y - s_z t_z)(v_y^+ - (s_x + s_z t_y)v_z^-)}{(1 - s_y t_y - s_z t_z)(1 - s_x t_x - s_z t_z) + (s_z + s_y t_x)(s_z - s_x t_y)}. \quad (\text{A.11})$$

Inserting this into  $v_z^+(v_x^-, v_y^-, v_z^-)$  then provides the expression for  $v_z^+ = v_z^+(v_x^+, v_y^+, v_z^-)$ .

## References

- [1] E. G. Harris, On a plasma sheath separating regions of oppositely directed magnetic field, *Il Nuovo Cimento* **23** (1962) 115.
- [2] D. Biskamp, E. Schwartz, and J. F. Drake, Two fluid theory of collisionless magnetic reconnection, *Phys. Plasmas* **4** (1997) 1002.
- [3] R. F. Lottermoser and M. Scholer, Undriven magnetic reconnection in magnetohydrodynamics and Hall Magnetohydrodynamics, *J. Geophys. Res.* **102** (1997) 4875.
- [4] M. A. Shay and J. F. Drake, The role of electron dissipation on the rate of collisionless magnetic reconnection, *Geophys. Res. Lett.* **25** (1998) 3759.
- [5] M. A. Shay, J. F. Drake, B. N. Rogers, and R. E. Denton, Alfvénic collisionless magnetic reconnection and the Hall term, *J. Geophys. Res.* **106** (2001) 3759.
- [6] X. Wang, A. Bhattacharjee, and Z. W. Ma, Scaling of Collisionless Forced Reconnection, *Phys. Rev. Lett.* **87** (2001) 265003.
- [7] J. D. Huba and L. I. Rudakov, Hall Magnetic Reconnection Rate, *Phys. Rev. Lett.* **93** (2004) 175003.
- [8] J. Büchner and J.-P. Kuska, Sausage mode instability of thin current sheets as a cause of magnetospheric substorms, *Ann. Geophys.* **17** (1999) 64.
- [9] R. Horiuchi and T. Sato, Three-dimensional particle simulation of plasma instability and collisionless reconnection in a current sheet, *Phys. Plasmas* **6** (1999) 4565.
- [10] P. L. Pritchett, Geospace Environment Modeling magnetic reconnection challenge: Simulation with a full particle electromagnetic code, *J. Geophys. Res.* **106** (2001) 3783.
- [11] P. L. Pritchett, Collisionless magnetic reconnection in a three-dimensional open system, *J. Geophys. Res.* **106** (2001) 25961.
- [12] M. Hesse, M. Kuznetsova, and J. Birn, Particle-in-cell simulations of three-dimensional collisionless magnetic reconnection, *J. Geophys. Res.* **106** (2001) 29831.
- [13] R. Sydora, Nonlinear dynamics of small-scale magnetic islands in high temperature plasmas, *Phys. Plasmas* **8** (2001) 1929.
- [14] P. Ricci, G. Lapenta, and J. U. Brackbill A Simplified Implicit Maxwell Solver, *J. Comp. Phys.* **183** (2002) 117.

- [15] P. Ricci, G. Lapenta, and J. U. Brackbill, GEM reconnection challenge: Implicit kinetic simulations with the physical mass ratio, *Geophys. Res. Lett.* **29** (2002) 2088.
- [16] A. Zeiler, D. Biskamp, J. F. Drake, B. N. Rogers, M. A. Shay, and M. Scholer, Three-dimensional particle simulations of collisionless magnetic reconnection, *J. Geophys. Res.* **107** (2002) 1230.
- [17] M. Scholer, I. Sidorenko, C. H. Jaroschek, R. A. Treumann, and A. Zeiler Onset of collisionless magnetic reconnection in thin current sheets: Three-dimensional particle simulations, *Phys. Plasmas* **10** (2003) 3521.
- [18] I. Silin, J. Büchner, Kinetic instabilities of thin current sheets: Results of two-and-one-half-dimensional Vlasov code simulations, *Phys. Plasmas* **10** (2003) 1299.
- [19] T. Wiegmann, J. Büchner, Evolution of magnetic helicity in the course of kinetic magnetic reconnection, *Nonlinear Processes in Geophysics* **8** (2001) 127.
- [20] J. Birn, J. F. Drake, M. A. Shay, B. N. Rogers, R. E. Denton, M. Hesse, M. Kuznetsova, Z. W. Ma, A. Bhattacharjee, A. Otto, P. L. Pritchett, Geospace Environmental Modeling (GEM) magnetic reconnection challenge, *J. Geophys. Res.* **106** (2001) 3715.
- [21] T. P. Armstrong, R. Harding, G. Knorr, D. Montgomery, Solution of Vlasov's equation by transform methods, *Advances in Computational Physics* **9** (1976) 29.
- [22] T. Arber, R. G. L. Vann, A critical comparison of Eulerian grid based Vlasov solvers, *J. Comp. Phys.* **180** (2002) 339.
- [23] F. Filbet, E. Sonnendrücker, P. Bertrand, Conservative numerical schemes for the Vlasov equation, *J. Comp. Phys.* **172** (2001) 166.
- [24] C. W. Nielson, H. R. Lewis, Particle-code models in the nonradiative limit, *Meth. Comput. Phys.* **16** (1976) 367.
- [25] P. L. Pritchett, F. V. Coroniti, R. Pellat, H. Karimadbadi Collisionless reconnection in two-dimensional magnetotail equilibria *J. Geophys. Res.* **96** (1991) 11523.
- [26] W. W. L. Lee, E. Startsev, Qin Hong, R. C. Davidson Electromagnetic (Darwin) model for three-dimensional perturbative particle simulation of high intensity beams. PACS2001, Proceedings of the 2001 Particle Accelerator Conference, IEEE Part vol. 3 (2001) 1906
- [27] C. K. Birdsall, A. B. Langdon, *Plasma Physics via Computer Simulation*, McGraw-Hill, New York, 1985.
- [28] F. Califano, A. Mangeney, C. Cavazzoni, P. Travnicek, A numerical scheme for the integration of the Vlasov–Maxwell system of equations, in: *Science and Supercomputing at CINECA, 2001*, p. 456.

- [29] C. Z. Cheng, G. Knorr, The integration of the Vlasov equation in configuration space, *J. Comp. Phys.* **22** (1976) 330.
- [30] O. Buneman, Time reversible difference procedures, *J. Comp. Phys.* **1** (1967) 517.
- [31] J. P. Boris, Relativistic plasma simulation-optimization of a hybrid code, in: *Proc. Fourth Conf. Num. Sim. Plasmas*, Vol. 3, 1970, p. 67.